

# The slip casting and mechanical characterisation of magnesium-alumino-silicate glass-ceramics

P. J. HOWARD, A. C. HUGHES

ALSTOM Research & Technology Centre, P O Box 30, Lichfield Road, Stafford, ST17 4LN, UK

E-mail: paul.howard@techn.alstom.com

An investigation of the slip preparation and casting of two magnesium-alumino-silicate glass powders has demonstrated the particular importance of the control of particle size distribution and slip viscosity in fabricating uniform glass-ceramics by powder methods. Measurement of strength and fracture toughness of fired material, coupled with particle size analysis and scanning electron microscopy has allowed interpretation of the quality of the material produced in terms of strength limiting flaws. Suggestions for the improvement of this type of material are made. © 1999 Kluwer Academic Publishers

## 1. Introduction

Glass-ceramics technology continues to interest the wider engineering community because of the unique combinations of physical properties which can be obtained in this type of material. Of particular interest in the recent past have been the developments of alkali-free glass-ceramics which have low dielectric constant and low loss at microwave frequencies and beyond. Such materials have been developed for, and used in, microwave packaging [1–3] and electromagnetic window [4, 5] applications.

Typical of these materials are magnesium-alumino-silicate glass-ceramics in which  $\alpha$ -cordierite is developed as the principal crystal phase. Dielectric constants less than 5 and loss tangents less than 0.0005 (at X-band) have been developed in various materials which span the range of thermal expansions from 2.5 to  $6 \times 10^{-6} \text{ K}^{-1}$ . Similar glass-ceramics made from slightly different starting compositions have been developed [6] in which MAS-Osumilite crystal phase is developed. These materials have similar dielectric properties, but have lower coefficients of thermal expansion being in the range from 1.5 to  $2.5 \times 10^{-6} \text{ K}^{-1}$ . Enstatite glass-ceramics (which were not included in this study) have higher expansions in the range 6 to  $12 \times 10^{-6} \text{ K}^{-1}$  [7].

If these materials are to achieve their commercial potential, in microwave applications for example, fabrication methods will be required which fulfil not only the physical properties already discussed, but also production at the right price of material having good mechanical and machining properties. Reliability and high yields of material in thin section (as 250  $\mu\text{m}$  substrates for example) demand high strength and fracture toughness. High  $Q$  in microstrip transmission lines demands low values of surface roughness of the dielectric substrate to reduce conductor loss.

In contrast with the better established bulk-route, the production of glass-ceramics from special glass pow-

ders has received greater attention in recent years [8, 9]. The particular attractions of the powder-route include broadening the range of physical properties which can be achieved, often by the incorporation of secondary particulate phases. Such inclusions might be added to modify thermal or dielectric properties by simple addition rules, or else may improve mechanical properties by more complex mechanisms. Additionally, special forming methods can be adopted for powder-route materials including tape-casting for thin sections and slip-casting.

Slip casting is one forming method which has received relatively little attention as a means of preparing glass powder compacts [10, 11], and this fact probably reflects the difficulties which are involved. Unlike clay particles (which are routinely slip-cast in the production of sanitary-ware), glass powders do not possess surfaces which naturally confer stability to their aqueous suspensions. In addition, glass powders are slow to mill by conventional methods and the resultant particle sizes tend to be relatively large, compared with commercial aluminas, say, being mainly in the range 1 to 10  $\mu\text{m}$  with mean size of 3–5  $\mu\text{m}$  and little sub-micron material. Thus glass powders present particular problems compared with naturally occurring silicates and refined oxide powders. Despite these difficulties the advantages of slip-casting are such that development in this area is justified.

The success of slip-casting depends almost exclusively on the production of well-dispersed and high-solids-content slips which can yield uniform green bodies. Such a green body is also a requirement for good mechanical properties in any sintered ceramic. Thus castable slips ought to lead to fired bodies which possess good mechanical properties by virtue of a uniform microstructure with few large pores which are homogeneously distributed.

Slip-casting is a very cheap process. Unlike other forming processes, for instance isostatic pressing, the

TABLE I Glass compositions selected for the study (mol.%)

Glass ref.	SiO <sub>2</sub>	Al <sub>2</sub> O <sub>3</sub>	MgO	BaO	B <sub>2</sub> O <sub>3</sub>	P <sub>2</sub> O <sub>5</sub>
F	72.00	14.00	13.33	0.67	-	-
H	56.9	15.6	24.5	-	2.0	1.0

capital costs amount to the purchase of a suitable mixer and a viscometer, the plaster mould being a cheap consumable item. The environmental costs are negligible since the process is water based and uses organic dispersants at very low concentrations [12].

In this study, slips were prepared of two magnesium-alumino-silicate glass powders: one  $\alpha$ -cordierite type, denoted H and one MAS-Osumilite type, denoted F. The compositions of the slips were related to their viscosities which, in turn, were related to density and uniformity of the fired bodies.

Of particular concern when slip casting technical ceramics is the achievement of uniform properties across the section of the fired body. Variation of the casting rate during the casting process might lead to variation in green density across the section of the body. In turn, this may lead to the generation of drying and firing stresses, resulting in strength-limiting flaws in the fired body. Such variation would be expected to affect most physical properties and particularly to reduce mechanical strength.

## 2. Experimental procedure

High-purity constituents were used in the melting of 1 kg batches of the glass compositions of Table I in a platinum crucible in an electric kiln at  $\sim 1600^\circ\text{C}$ . The melts were homogenised by a combination of swirling and fritting and finally fritted in cold, filtered tap water. The frit was dried then dry-ball-milled for 4 hours using 25 mm alumina balls (1 kg of frit in a 5 l porcelain jar with 50 vol.% of alumina balls). The resulting coarse powder was passed through a  $75\ \mu\text{m}$  sieve. The sub- $75\ \mu\text{m}$  glass powder was then wet-ball-milled in porcelain jars with 18 mm alumina balls and water. Typically, 350 g of powder was wet-ball-milled at 68 wt.% solids content in a 1 litre jar for 48 hours. Sufficient Dolapix ET85\* dispersant was added to maintain a near-optimum viscosity for efficient milling. The viscosity of the slip after 48 hours milling was greater than that required for slip-casting so it was modified by the addition of water and/or further dispersant and divided into several lots in preparation for further modification and slip-casting experiments. The main experimental variables were to be solids content and dispersant concentration. The pH of the slips was adjusted to be within the range recommended for the particular dispersant used.

Dolapix ET85 was added on a solids to solids basis from an aqueous solution of known composition. In order to suppress the tendency of the slips to foam, an anti-foaming agent - Contraspuum\* - was added in small amounts. The viscosity of the slips was measured at room temperature using a cone and plate vis-

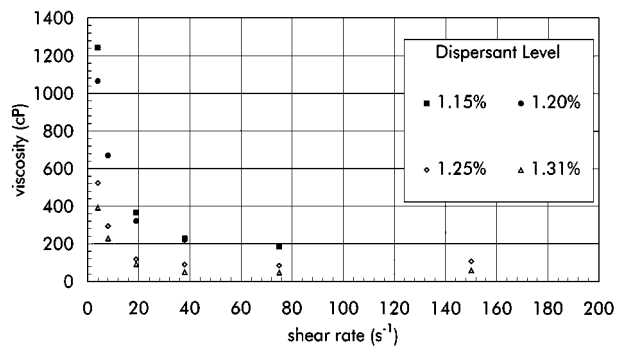


Figure 1 Viscosity v. shear rate for slips of material F, at 65 wt.% solids loading.

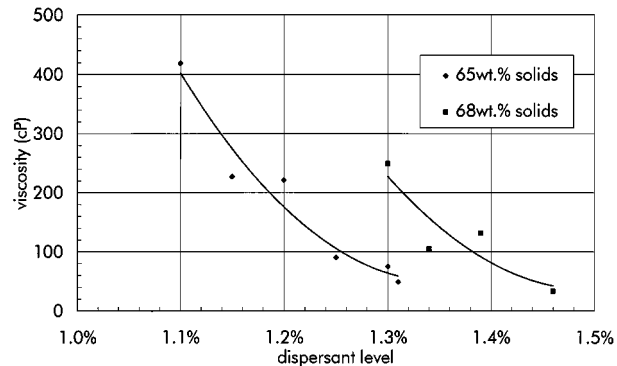


Figure 2 Viscosity v. dispersant level for slips of material F, at 65 wt.% and 68 wt.% solids loadings.

cometer<sup>†</sup> over a range of shear rates from 1–200  $\text{s}^{-1}$ . Fig. 1 shows the shear rate dependence of slips of 65 wt.% solids content and various dispersant concentrations and in Fig. 2, the viscosity at a shear rate of  $38\ \text{s}^{-1}$  is plotted against dispersant concentration for 65 wt.% and 68 wt.% solids contents slips. (Note that this data was for the MAS-Osumilite slips, denoted F).

An experiment was conducted in which  $\varnothing 31\ \text{mm}$  hollow, closed-ended cylinders were produced by drain-casting from plaster moulds<sup>‡</sup>. The experimental variables were the slip composition and its viscosity and the plaster : water ratio of the mould and its free water content. For a given set of variables, several drain-cast bodies were produced over a range of drain times. The wall thickness and diameter of each cast body was measured before drying and firing. The firing shrinkage and fired density were measured and used to calculate the green density.

## 3. Slip-casting results

Data was analysed from the drain-casting of about thirty different slips. According to a model described in ref. 12, the thickness of the cast layer,  $\varepsilon$ , is a parabolic function of the drain time,  $t$ , for homogeneous bodies. That is, uniform green density is observed in bodies whose casting obeys this law. Therefore, in this work, the casting rate was defined as the gradient of the linear plots of cast thickness,  $\varepsilon$  versus the square root of the drain time,  $t^{1/2}$ .

<sup>†</sup> Brookfield Inc.

<sup>‡</sup> Pottery Plaster, ex British Gypsum Ltd.

\* Zschimmer & Schwartz GmbH & Co.

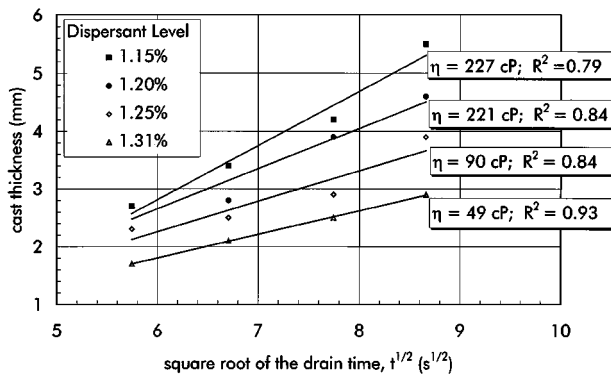


Figure 3 Cast thickness v. square root of drain time for slips of material F at 65 wt.% solids loading.

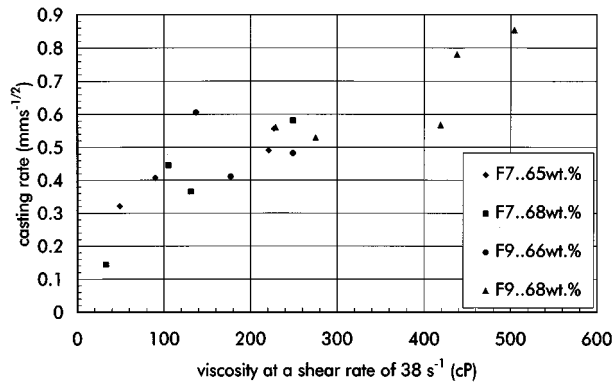


Figure 4 Casting rate v. viscosity for slips of two particle size distributions and solids loadings.

Fig. 3 shows linear plots of the cast thickness,  $\varepsilon$ , against root drain time for 65 wt.% solids loading slips for a range of dispersant concentrations. The legend also gives the viscosity of the slips and the correlation coefficient,  $R^2$ , extracted from the line fitting. A higher value of  $R^2$  indicates a better linear fit and this was related to uniformity across the cast section. The gradients of these curves (casting rates) can be seen to fall with increasing dispersant concentration (and decreasing viscosity). Additionally, the plots become more linear with decreasing viscosity, thus suggesting greater uniformity within the green body. This result was observed in all cases.

Casting rate versus viscosity was plotted for four slips (of two particle size distributions and two solids loadings), Fig. 4. Allowing for a small amount of scatter, the data points fall on the same straight line and this indicates that slip viscosity is the main determinant of casting rate. Fig. 5 shows an inverse relationship between green density and casting rate for two powders and two solids loadings. The significance of these observations for glass powders lies in the fact that they are generally more coarse than other technical ceramics. Thus to achieve slow casting rates, and therefore higher green density, requires the preparation of particularly low viscosity slips.

#### 4. Mechanical and microstructural characterisation of fired bodies

Low viscosity slips of F and H glass powders, each of various particle size distributions, were cast into rectan-

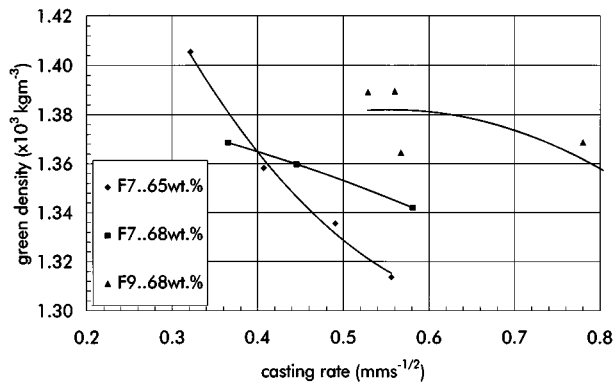


Figure 5 Green density of slip-cast bodies v. casting rate.

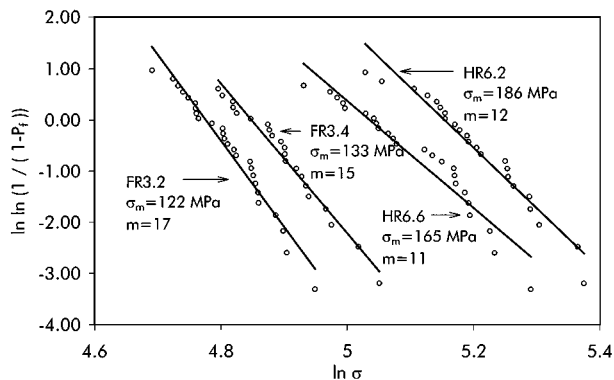


Figure 6 Weibull plot of representative materials.

gular plaster moulds to a thickness of 10–15 mm. The cast blocks were removed from the moulds within one hour of casting and allowed to dry at ambient conditions for 16 hours, then at 50°C for four hours. Firing was performed at a rate of 2 or 5 K min<sup>-1</sup> to 1000°C (material H) and 1150°C (material F) with soaks from 2 to 10 h.

Measurements of strength and fracture toughness were made on rectangular bars which were cut from the fired blocks of  $\alpha$ -cordierite material (H) and MAS-Osumilite material (F). Each strength sample contained more than thirty specimens, each of which was measured in three-point flexure with a span of 20 mm. The fracture toughness specimens were single-edged, notched-beams (SENB), also measured in three-point flexure.

Fig. 6 is a plot of  $\ln \ln(1 / P_f)$  versus  $\ln \sigma$  for representative samples of material F and H. In this Weibull plot,  $P_f$  is the failure probability of the sample at a given applied stress,  $\sigma$ , and the gradient represents its Weibull modulus. It can be seen that generally, the H material was the stronger and that it had the larger Weibull modulus.

The fracture toughness values of the H materials were in the range 1.9 to 2.2 MPa·m<sup>1/2</sup> and those of the F materials were in the range 1.6 to 2.1 MPa·m<sup>1/2</sup>. The strength and fracture toughness results were used to calculate a characteristic flaw size,  $C$ , for each of the materials according to the following Griffith energy balance equation.

$$C^{1/2} = \frac{K_{IC}}{\pi \sigma_f}$$

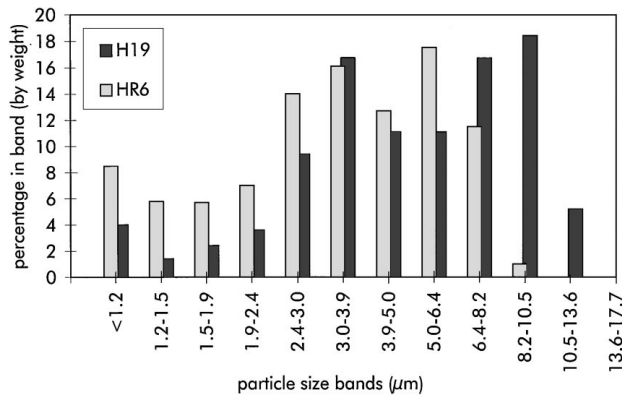
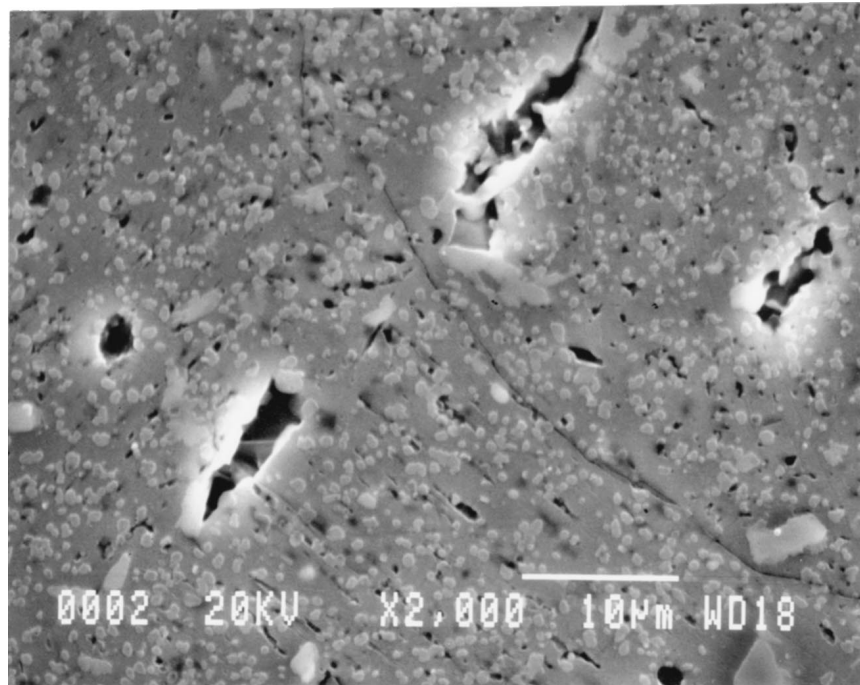


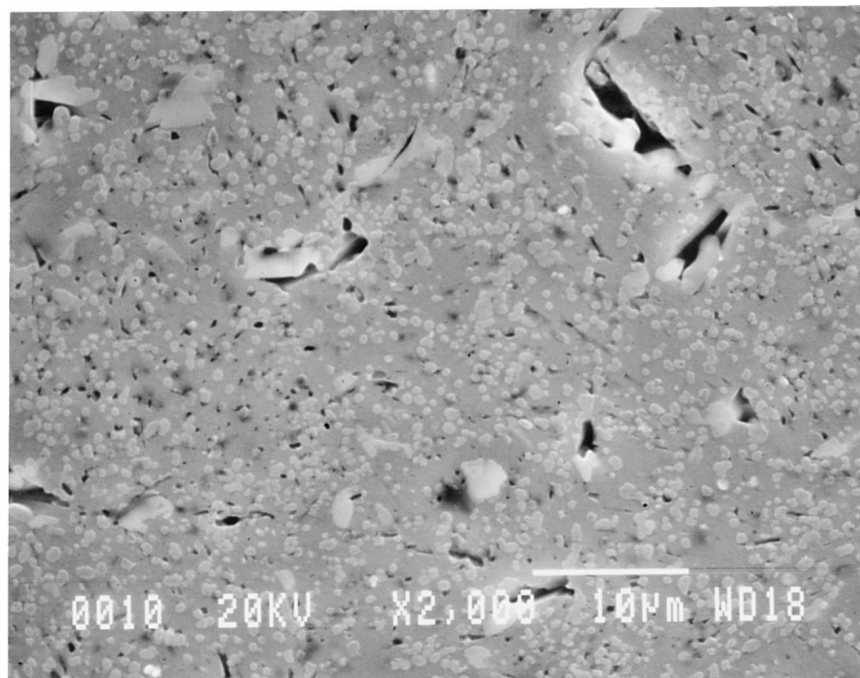
Figure 7 Particle size distributions of the powders H19 and HR6.

where  $K_{IC}$  = critical stress intensity factor (fracture toughness);  $\sigma_f$  = flexural strength;  $\pi$  = a nominal geometrical term. Whilst the numerical value of  $C$  is not taken as a precise measure of crack length because of uncertainty in the geometrical term, it nevertheless gives a meaningful relative value which is useful in comparing materials and in making correlations with processing conditions.

In glass-ceramics denoted H, the size of the critical flaw did not seem to be dependent on firing schedule. Comparison of samples processed at different heating rates and to different temperatures showed critical flaws to be related to the particle size distribution of their respective starting powders. Two HR6 samples had



(a)



(b)

Figure 8 Scanning electron micrographs of polished sections of two slip-cast materials, (a) H19/1.5 and (b) HR6.2.

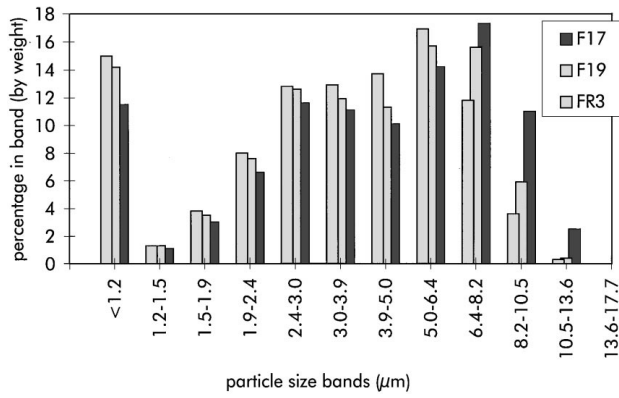
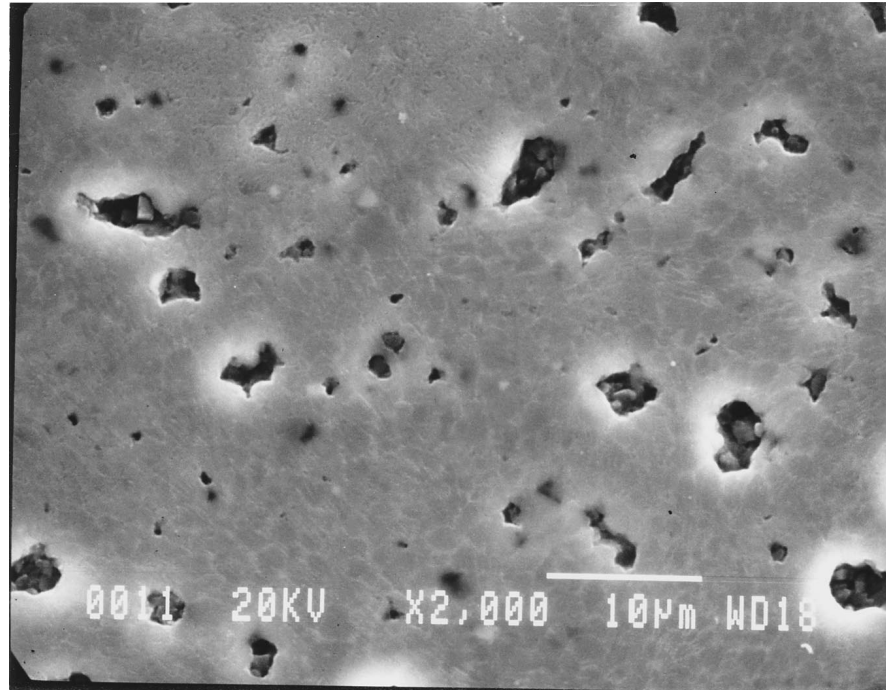


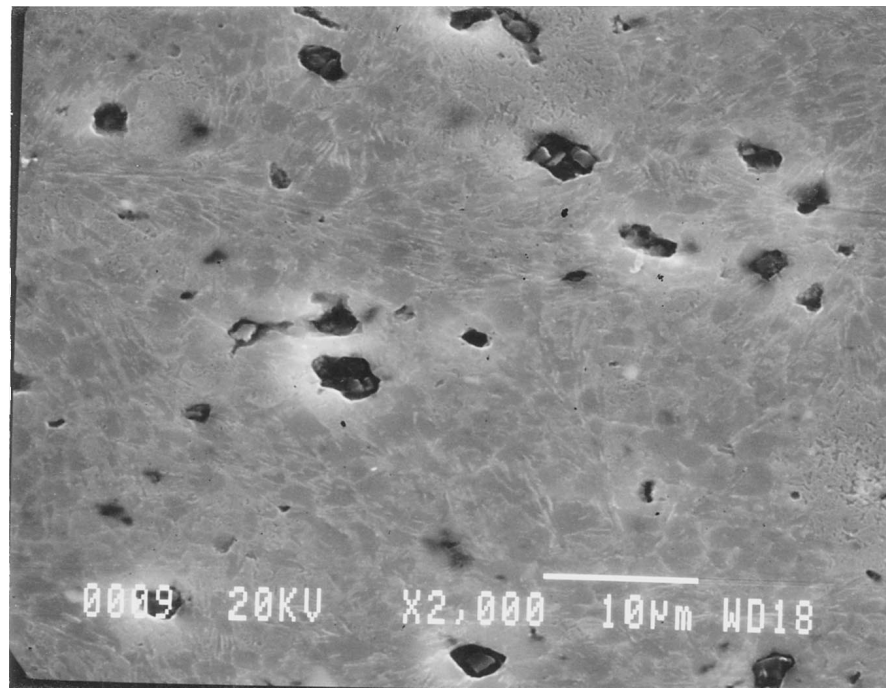
Figure 9 Particle size distributions of the powders F17, F19 and FR3.

critical flaws which were about half the size of those of the two H19 samples. Fig. 7 shows the particle size distributions of the powders H19 and HR6 from which these samples were prepared and Fig. 8a and b show  $\times 2000$  scanning electron micrographs of polished sections of representative, fired bodies. The micrographs confirm that the largest pores in the H19 material are larger than those in the HR6 material.

Both particle size distributions show a tri-modal form. In H19 the distribution at the large particle size end is centred on  $11 \mu\text{m}$ , whereas in HR6, the corresponding mean is at  $7 \mu\text{m}$ . The intermediate distribution for both powders is centred on  $4.5 \mu\text{m}$  and the proportion of sub-micron powder was about 8% in each. The



(a)



(b)

Figure 10 Scanning electron micrographs of polished sections of two slip-cast materials, (a) F19/M1 and (b) FR3.2.

evidence suggests that, in the glass-ceramics denoted H, the particle size distribution of the larger fraction of powder plays the dominant role in determining the critical flaw size and thus determines the strength of the material.

Of the type F glass-ceramics, the size of the critical flaw was 50% bigger in samples processed at  $5 \text{ K min}^{-1}$ , compared with those processed at  $2 \text{ K min}^{-1}$ . Also, in common with type H materials, the critical flaw size varied between samples made from different starting powders which had been processed to the same heat-treatment schedule, although this effect was less marked for type F. Fig. 9 shows the particle size distributions of the powders, F17, F19 and FR3. It can be seen that, in this series, the powders became progressively finer over a narrow range. In particular, the mean particle size of the population at the larger end of the range changed from  $9 \mu\text{m}$  in F17 to  $7 \mu\text{m}$  in FR3. This change reflects the progressive fall in critical flaw from  $76 \mu\text{m}$  (in F17) to  $61 \mu\text{m}$  (in FR3). Comparison of scanning electron micrographs of F19/M1 and FR3.2 (Fig. 10a and b, respectively) reveals that the largest pores in the former are in the  $6\text{--}8 \mu\text{m}$  range whereas in FR3.2 the corresponding pores are  $4\text{--}5 \mu\text{m}$ .

The implication is that, to produce stronger glass-ceramics of these compositions, attention ought to be focused on powder preparation including quenching of the glass melt and milling. The results suggest that a substantial decrease in mean particle size at the large end of the range ought to yield type H glass-ceramics with strengths up to 250 MPa and type F materials up to 200 MPa.

## 5. Conclusions

Powder processing of alkali-free glass powders has been demonstrated to yield potentially useful materials for microwave applications such as substrates, packaging and radomes. Whilst the dielectric properties of these materials are important, they will not be widely

used unless they can be processed reliably and utilised with confidence. In this work it has been shown that strong and reasonably tough materials can be fabricated from slips which contain properly dispersed powders. It has been demonstrated that, for the material types of this study, particle size distribution and slip viscosity are the most important determinants of material quality. The findings of this study should apply equally to tape-cast material.

## Acknowledgements

The authors wish to acknowledge the assistance of colleagues at ALSTOM Research & Technology Centre, in particular Trevor Hales, for their contributions to technical discussions during the course of this work. We are grateful, also, to the UK MoD and to ALSTOM for its permission to publish this paper. This work was carried out with the support of the Defence and Evaluation Research Agency, DERA (Malvern).

## References

1. R. R. TUMMALA, *J. Am. Ceram. Soc.* **74** (1991) 896.
2. N. E. PRIESTLEY, *Glass Technology* **31** (1990) 7.
3. G. PARTRIDGE, C. A. ELYARD and H. D. KEATMAN, *ibid.* **30** (1989) 215.
4. D. LEWIS and J. R. SPANN, in Proc. 15th Conf. Electromagnetic Windows, 1980, p. 165.
5. J. B. KOUROUPIS, *John Hopkins APL Technical Digest* **13** (1992) 386.
6. W. WINTER *et al.*, *Glastech Ber.* **66** (1993) 109.
7. M. I. BUDD, *J. Mater. Sci.* **28** (1993) 1007.
8. R. MORRELL, *Proc. Brit. Ceram. Soc.* **28** (1979) 53.
9. E. M. RABINOVICH, *Adv. Ceram.* **4** (1982) 327.
10. V. A. BEVZ and T. M. KHRANOVSKAYA, *Steklo I Keramika* **7** (1991) 2.
11. A. M. AKH'YAN, *Steklo I Keramika* **5** (1991) 27.
12. C. H. SCHILLING, "Engineered Materials Handbook, Vol. 4" (ASM International, 1991) p. 153.

Received 24 August 1999

and accepted 28 March 2000